Insights into Synergistic Effects of Counterion and Ligand on Diastereoselectivity Switch in Gold-Catalyzed Post-Ugi Ipso-Cyclization

Jun He,[||] Jie Zhang,[||] Yunhe Li,[||] Yan-bo Han, Mengyang Li, and Xiang Zhao*

Read Online

ACCESS | Metrics & More | Article Recommendations | SI Supporting Information

ABSTRACT: The concept of diastereoselectivity switch in gold catalysis is investigated, which primarily depends on the effects of ligand and counterion. The origins of gold-catalyzed post-Ugi ipso-cyclization for the diastereoselective synthesis of spirocyclic pyrrol-2-one-dienone have been explored with density functional theory calculations. The reported mechanism emphasized the importance of the cooperation of ligand and counterion in diastereoselectivity switch, leading to the stereocontrolling transition states. Furthermore, the nonbonding interactions primarily between the catalyst and the substrate play a significant role in the cooperation of ligand and counterion. This work would be useful to further understand the reaction mechanism of gold-catalyzed cyclization and the effects of ligand and counterion.
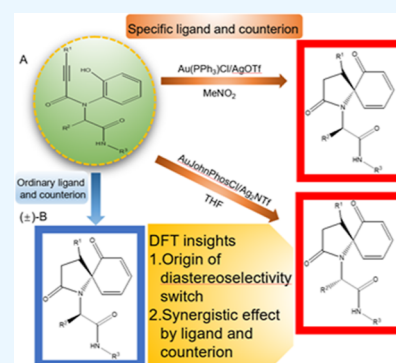
INTRODUCTION

Spirocycles play an important role in drug discovery and development owing to their inherent three-dimensionality and structures.[1−3] Furthermore, the preparation of spirocycles in enantio- and diastereomerically enriched forms is of great significance in the pharmaceutical industry and materials science.[4] Dearomatization is an effective method to synthesize three-dimensional molecular scaffolds. Dearomatization strategies in a multicomponent fashion often result in complex heterocyclic scaffolds, which have attracted the attention of the synthetic organic community due to their great significance in asymmetric catalysis.[5−7] Importantly, asymmetric catalysis has been recognized as the most enabling strategy for accessing spirocycles in enantio-enriched forms.[8] Therefore, it is pertinent to mention that the development of novel post-MCR (multicomponent reaction) transformations for complex polycyclic molecular scaffolds is rather significant and interesting.[9]

Notably, catalyst optimization including gold catalysis is as frustrating as it is compulsory.[10,11] Specifically, ligands have played a crucial role in advancing homogeneous gold catalysis.[12−17] Alternatively, the metal counterions proved to be of pivotal importance in impacting both the reaction mechanism and the regioselectivity of gold-catalyzed transformations.[18−20] On the other hand, most of the approaches that employ gold complexes as catalytic systems are sustainable from a green chemistry perspective.[21] Encouraged by these important results, we further explored the use of gold-catalyzed dearomatization in the formation of spirocycles for understanding the remarkable stereoselectivity.

More importantly, data science and physical organic chemistry are integral to identifying and understanding the key connections and patterns hidden within the data and accelerating our fundamental understanding of chemical reactions and reactivity.[22−25] Nevertheless, Durand and Fey demonstrated the applications in different aspects of catalyst design in combination with computational mechanistic studies and thus describe the process of their journey toward truly predictive models in the homogeneous organometallic catalysis.[26]

The four-component Ugi reaction is one important platform for obtaining various precursors for diversity-oriented synthesis.[27] The synthesis of bioactive natural products or versatile synthons via tuning of the gold catalytic system is also developing fast.[28] In 2012, van der Eycken et al. reported a method for the synthesis of indoxazosin using Ugi products as reactants followed by gold-catalyzed intramolecular hydroformylation, which has a unique diastereoselectivity.[29] In more detail, the Ugi adduct catalyzed by gold results in the final spiroindoline product, which are the merits of this approach. Later, they successfully developed an efficient diversity post-Ugi gold-catalyzed domino cyclization for the synthesis of

tetracyclic scaffolds, which exhibit good yields as well as full diastereoselectivity.[30] Computational experiments have identified that in such kinds of reactions, counterions play a critical role in inducing multiple selectivity through a concerted or cascade mechanism.[31,32] In 2018, van der Eycken and coworkers described a gold-catalyzed post-Ugi ipso-cyclization for the diastereoselective synthesis of spirocyclic pyrol-2-one-dienones (Scheme 1).[33] Importantly, the diastereoselectivity

Scheme 1. Gold-Catalyzed Post-Ugi Ipso-Cyclization Described by van der Eycken;[33] [Reproduced from *J. Org. Chem.* 2018, 83(15), 8170−8182. Copyright 2018 American Chemical Society]
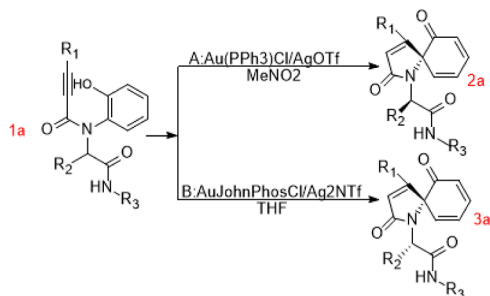
switch is modulated by the appropriate catalytic system. The production of diastereoselectivity is different from chiral induction, similar to asymmetric synthesis (the interaction between the initial chiral center and the reaction conditions results in diastereoselectivity). This novel strategy is useful for designing and optimizing stereoselective metal-catalyzed transformations.[34] The involvement of the diastereoselectivity switch controlled by the synergistic effect of ligand and counterion on gold catalysis has particularly attracted our attention.[35] In gold-catalyzed dearomatization reactions, the absence of a comprehensive mechanistic understanding has hindered the rational selection of counterions and ligand, which is still empirical.[36] Further mechanistic studies and novel control experiments are needed for a deeper understanding of the role of additives in gold catalysis.[37] Computational chemistry has made a sustained contribution to the understanding of the detailed reaction mechanism and regioselectivity in organic reactions.[38] For example, the transition states and intermediates contributing to the transformation of reactants into desired and undesired products can now be

determined, including their geometries, energies, charges, etc.[39−43] Here, density functional theory computations are carried out to further understand the origin of the diastereoselectivity switch in gold-catalyzed post-Ugi ipso-cyclization (Scheme 1),[33] and a relevant mechanism diagram (Scheme 2) is revealed through theoretical calculations.

■ COMPUTATIONAL DETAILS

All calculations in this study were conducted using the Gaussian 16 program package.[44] The geometries of all species were fully optimized by density functional theory (DFT) with the M06 and 6-31G(d,p)[45] basis set for all atoms, except for Au;[47,48] and the Lanl2DZ(f) basis set was applied for Au.[46] Vibrational frequency calculations conducted at the M06/6-31G(d,p) theoretical level were used to characterize the minimum points (free from imaginary frequencies) or TS points (with only one imaginary frequency). In several significant cases, calculation of intrinsic reaction coordinates[47] was performed to unambiguously connect the TS with the reactants and products. The relative energies were corrected including the vibrational zero-point energies. In order to obtain much more exact energy profiles, the single-point energies were calculated at the M06/Lanl2TZ(f)∼6-311G(d,p) level of theory where Lanl2TZ(f) is used for the Au atom and the 6-311G(d,p) basis set is used for the other atoms, and the single-point energies including the solvation effect of THF or CH_3NO_2 were also calculated at the M06/Lanl2TZ(f)-6-311G(d,p) level.[48] Graphical representations of optimized geometries were created by using CYLView.[49] The non-covalent interaction (NCI) study was performed with Multiwfn.[50] All of the NCI isosurfaces were presented by using VMD version 1.9.3.[51]

■ RESULTS AND DISCUSSION

General Consideration. According to the experimental results,[33] the reaction goes through metal gold coordination, dearomatization to form spiro rings, and final dissociation to form the product. In their controlling experiments, the proto-demetallation step is an irreversible step[33] (**2inta** to **2a** or **3inta** to **3a**, as shown in Scheme 2), and the calculations of the ring closing step and the proto-demetallation step of the condition c (PAu(PPh$_3$)OTf) indicate that the energy barrier of the proto-demetallation step (the 24.6 kcal/mol of **4tsc** and the 23.6 kcal/mol of **5tsc**) is much higher than that of the ring

Scheme 2. General Mechanistic Scheme for the Gold(I)-Catalyzed Ipso-Cyclization
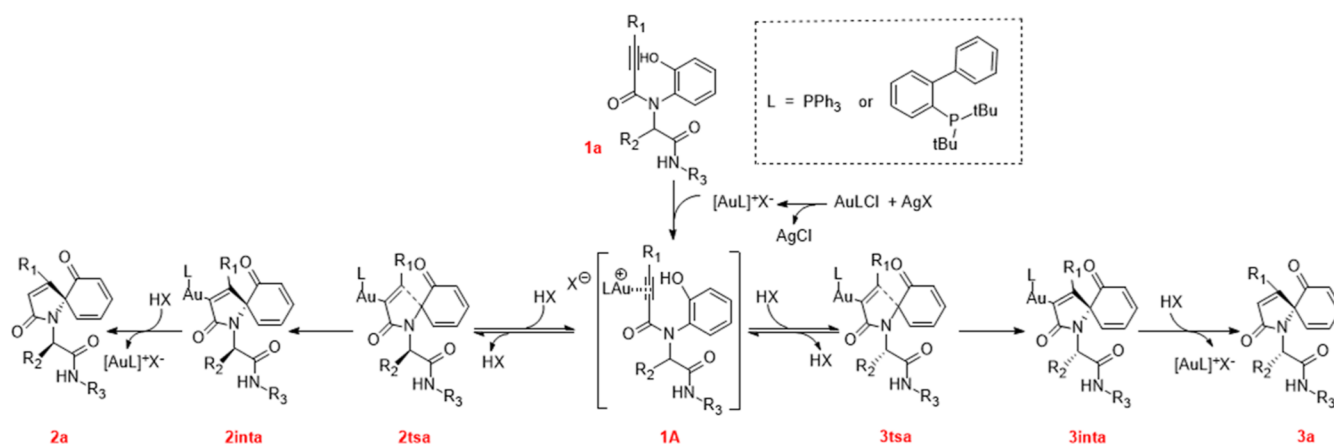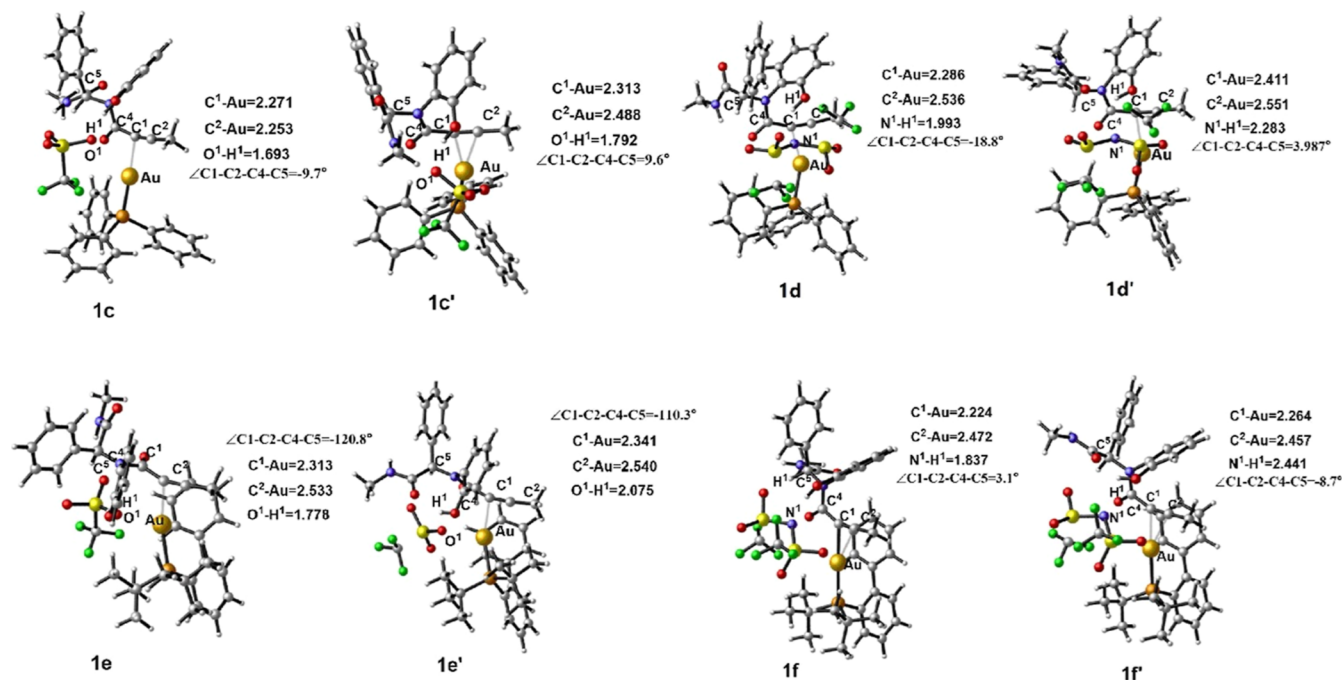
Figure 1. Optimized geometries for the primary coordination mode of substrate 1, with ligands and counterions of [PPh$_3$AuOTf] (**1c**/**1c′**), [PPh$_3$AuNTf$_2$] (**1d**/**1d′**), [JohnPhosAuOTf] (**1e**/**1e′**), and [JohnPhosAuNTf$_2$] (**1f**/**1f′**).

closing step (6.2 and 13.7 kcal/mol) (Figure S1). Therefore, the proto-demetallation step can be confirmed as a rate-determining step. Meanwhile, the energy barriers of two proto-demetallation steps are similar, which indicates that the proto-demetallation step may not determine the diastereoselectivity. Thus, we speculate that the diastereoselectivity of the reactions is determined in the ring closing step (**1A** to **2inta** or **3inta**, as shown in Scheme 2), and we mainly investigated the ring closing step. Furthermore, diastereomers have different conformations of the initial chiral center rather than the second chiral center after ring closure. The initial chiral center does not produce any chemical changes, but the reaction conditions can control the diastereoselectivity. The initial chiral center should control the diastereoselectivity together with the reaction conditions. Therefore, we start with the reactants with different conformations. In the stereocontrolling intramolecular spiro-cyclization step, the product can exist as either the **2a** or **3a** isomer (Scheme 1). We explored the conformations for each of these possible structures and then predicted the diastereoselectivities.

Energy Profiles for the Synthesis of Vinyl Gold(I) Intermediates. The selectivity of other gold-catalyzed multicomponent de-aromatic domino cyclization reactions can be regulated by ligands; therefore, we first calculated the ring closing step in the case of only ligands. The two ligands used in the experiment (L$_1$ = PPh$_3$, L$_2$ = JohnPhos) were used to investigate the step of dearomatization to form spiro rings in the presence of a single ligand. The calculated results did not show the diastereoselectivity as shown in the experiment. Therefore, counterions play a key role in the regulation of diastereoselectivity.

The geometry and electronic properties of the primary structures of substrate 1 with different ligands and counterions (**1c**/**1c′**, **1d**/**1d′**, **1e**,**1e′**, and **1f**/**1f′**) are presented in Figure 1. The reaction starts from the substrates with different initial configurations, uses the ligands and counterions used in the

experiment to obtain the reactants **1c**/**1c′** and **1f**/**1f′**, and cross combines the ligands and counterions in the experiment to obtain the reactants **1d**/**1d′** and **1e**/**1e′**. **1**/**1′**(**1c**/**1c′**, **1d**/**1d′**, **1e**,**1e′**, **1f**/**1f′**), two initial complexes between the gold-complex [L−Au−X] and the reactant with the chiral center (C4), are the starting points of the diastereo-divergent spiro-cyclization, respectively, which are controlled by activation mode. For comparison, the zero-energy reference point of the reaction is set as 1 (**1c**, **1d**, **1e**, and **1f**).

To gain a better understanding of the activation mode and origin of the synergy effect between counterion and ligand-mediated catalytic cycles, we calculated the energy profiles for [PPh$_3$AuOTf] (Figure 2a), [JohnPhosAuNTf$_2$] (Figure 2b), [PPh$_3$AuNTf$_2$] (Figure 2c), and [JohnPhosAuOTf] (Figure 2d). The reactants are racemic, and the energies of the two different chiral isomers are the same. However, as observed with the combination of ligands and counterions with the reactants, there are great energy differences between the different chiral reactants. Thus, the observed diastereoselectivity for the reaction with a different [L−Au−X] complex can be rationalized by comparing the relative energies of **1c−f** vs **1c′−f′**. The free energy difference $\Delta\Delta G^{\ddagger}$ catalyzed by PPh$_3$AuOTf between **1c** and **1c′** is calculated to be 8.0 kcal/mol ($\Delta G_{1c} - \Delta G_{1c'}$); **1c′** is more stable than **1c**, and the reaction tends to produce reaction intermediates **3intc** instead of **2intc**. For the JohnPhosAuNTf$_2^-$ catalyzed reaction, the free energy between **1f** and **1f′** is calculated to be −9.1 kcal/mol ($\Delta G_{1f} - \Delta G_{1f'}$). **1f** is more stable than **1f′**, the reaction tends to produce reaction intermediates **2intf** instead of **3intf**. These are consistent with the experimental results. In addition, according to the Curtin−Hammett principle, the diastereoselectivity of the model reaction is controlled by the competition between the competing diastereoselectivity-determining transition states. Thus, the observed diastereoselectivity for the reaction with a different [L−Au−X] complex can be rationalized by comparing the relative energies of **2tsc-f** vs
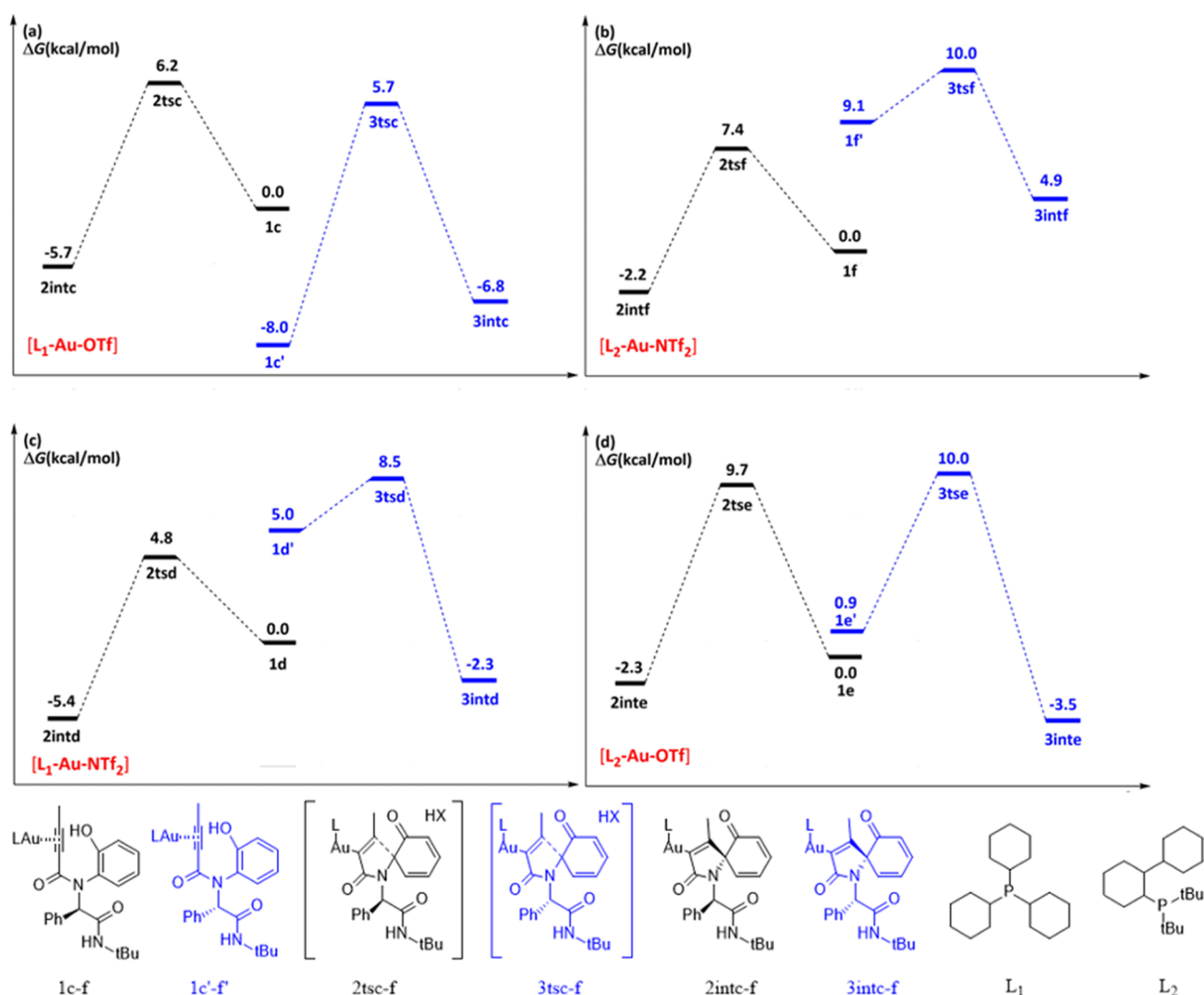
Figure 2. Comparison of the energy profiles associated with different ligands and counterions for L_1-Au-OTf (a), L_2-Au-NTf$_2$ (b), L_1-Au-NTf$_2$ (c), and L_2-Au-OTf (d). **1c−f** and **1c′−1f′** are reactants. **2tsc-f** and **3tsc-f** are reaction transition states. **2intc-f** and **3intc-f** are reaction intermediates.

3tsc-f. The rate-determining activation barrier difference $\Delta\Delta G^*$ catalyzed by Ph$_3$AuOTf between **2tsc** and **3tsc** is calculated to be 0.5 kcal/mol ($\Delta G_{2tsc} - \Delta G_{3tsc}$), which is in line with the experimentally observed diastereoselectivity. For the JohnPhosAuNTf$_2$-catalyzed reaction, the rate-determining activation barrier difference between **2tsf** and **3tsf** is −2.6 kcal/mol ($\Delta G_{2tsf} - \Delta G_{3tsf}$), which is in qualitative agreement with the experimental observation. These results are corroborated by the analysis of the reactants. Therefore, the combination of ligands and counterions can realize the diastereoselective synthesis of products, and the diastereoselectivity of different combinations is different. As discussed above, an interplay between ligand and counterion could occur in gold-catalyzed post-ugi ipso-cyclization. A synergistic effect by these factors could solve the dilemma that existed in homogeneous catalysis, which may pave the way toward bulk and green catalysis with gold. Van der Eycken and co-workers' work has well demonstrated this concept via experimental findings. We first investigated the synergistic effect by these factors based on computational catalysis for organic synthesis. These computational results in this work described are remarkable as they suggest that sustainable and stereoselectivity switch can be achieved with homogeneous gold catalysis. Therefore, this

work will help researchers to look at this promising area from different perspectives with respect to optimization of catalysts and conditions in gold catalysis.

In contrast, for the catalytic system JohnPhosAuOTf-catalyzed reaction (Figure 2d), the free energy between **1e** and **1e′** is calculated to be −0.9 kcal/mol ($\Delta G_{1e} - \Delta G_{1e'}$), thus indicating a lower diastereoselectivity. Therefore, only a specific combination of ligands and counterions can produce diastereoselectivity. These energy data have a good correlation with the geometric parameters of the reactant structures (Figure 1). Intriguingly, the flexible electron-deficient PPh$_3$ ligand favors combination with OTf$^-$ (high hydrogen bond basicity), and the bulky electron-abundant JohnPhos ligand favors combination with NTf$_2^-$ (low hydrogen bond basicity). The geometrical details are used to visualize the unique diastereo-divergent reactivity (Figure 3). Clearly, it can be seen that the combination of small ligand and small counterion as well as the combination of large ligand and large counterion can all show good diastereoselectivity. This is consistent with van der Eycken's observation that the synergy of both counterion and ligand is essential for highly diastereoselective switchable control.[33] We speculate that the different non-covalent interactions between different reaction conditions and
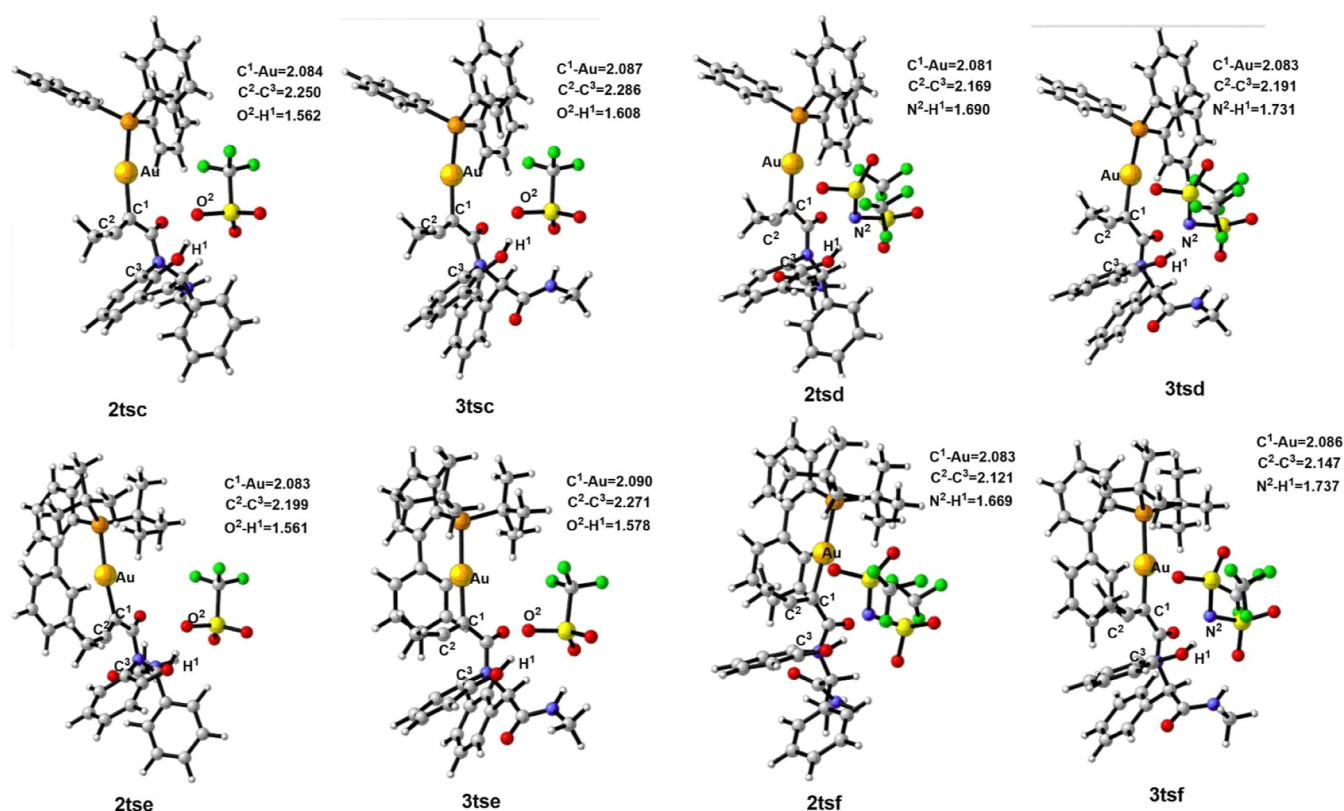
Figure 3. Optimized geometries of some key transition structures, with ligands and counterions of [PPh$_3$AuOTf] (**2tsc/3tsc**), [PPh$_3$AuNTf$_2$] (**2tsd/3tsd**), [JohnPhosAuOTf] (**2tse/3tse**), and [JohnPhosAuNTf$_2$] (**2tsf/3tsf**).

initial reactants lead to the nonenantioselectivity of the reaction.

Origin of Diastereoselectivity. Owing to the current research endeavors in the fields of homogeneous catalysis,[52] innovative materials,[44,53] and petrochemical research,[54] significant interest in weak noncovalent interactions has been steadily growing, as these interactions are the driving forces. Importantly, noncovalent interactions enable the rapid identification of attractive and repulsive noncovalent interactions from promolecular densities.[54] Many examples are provided with regard to how this new twist enables the characterization and retrieval of local information in supramolecular chemistry and transition metal catalysis at the static and dynamic levels.[55] In order to understand how the combination of large ligand and large counterion as well as small ligand and small counterion controls the diastereoselectivity, NCI analysis of the eight reactants (**1c**−**1f**, **1c′**−**1f′**) was performed, and the corresponding weak interaction diagrams were obtained (Figure 4). The counterion and chirality of the two reactants are shown in Figure 4 (**1c** and **1c′**), and the interaction between the counterions and the chiral center is different. The counterion in **1c** is close to the side of the benzene ring, and the counterion has a hydrogen bond with the active proton, but there is basically no interaction with the benzene ring. The counterion in **1c′** is close to the side of the amide group. It has a hydrogen bond with the hydrogen ion on the amide group, stabilizing **1c′**. The counterion and chirality of the two reactants are shown in Figure 4 (**1f** and **1f′**), and the weak interaction between the counterions and the chiral center is different. Compared with **1f′**, in **1f**, the counterion has a hydrogen bond with the

benzene ring, stabilizes **1f**, and thus produces diastereoselectivity.

Furthermore, the combination of the large ligand and the small counterion does not affect the interaction between the counter ion and the chiral center, as shown in Figure 4 (**1e** and **1e′**), so it does not show divergent diastereoselectivity in experiment.[33] The situation in Figure 4 (**1d** and **1d′**) is similar to that in Figure 4 (**1e** and **1e′**), but due to the existence of small ligands, there is a weaker interaction between the counterion and the ligand; therefore it also indicates the presence of diastereoselectivity. These results are also consistent with the previous reaction energy changes. Compared with Figure 4 (**1c** and **1c′**) and Figure 4 (**1e** and **1e′**), the interaction between counterion and the initial chiral center is similar, but the interaction between counterion and ligand is different. As observed in Figure 4 (**1e** and **1e′**), the small counterions are far away from the ligand and have no interaction with the substrate; therefore, there is no diastereoselectivity. Compared with Figure 4 (**1d** and **1d′**) and Figure 4 (**1f** and **1f′**), there is interaction between large ligand and large counterion, but there is no interaction between small ligand and large counterion. Therefore, the interaction between different ligand and counterion combinations and reactants determines the diastereoselectivity, and the combination of small ligand and small counterion as well as large ligand and large counterion has more advantages. The NCI analysis revealed that the nonbonding interactions were responsible for governing the diastereoselectivity switch in gold-catalyzed ipso-cyclization.

Origin of the Diastereoselectivity Switch. The general understanding of the gold-catalyzed dearomatization obtained further inspired us to explore the effect of the interplay
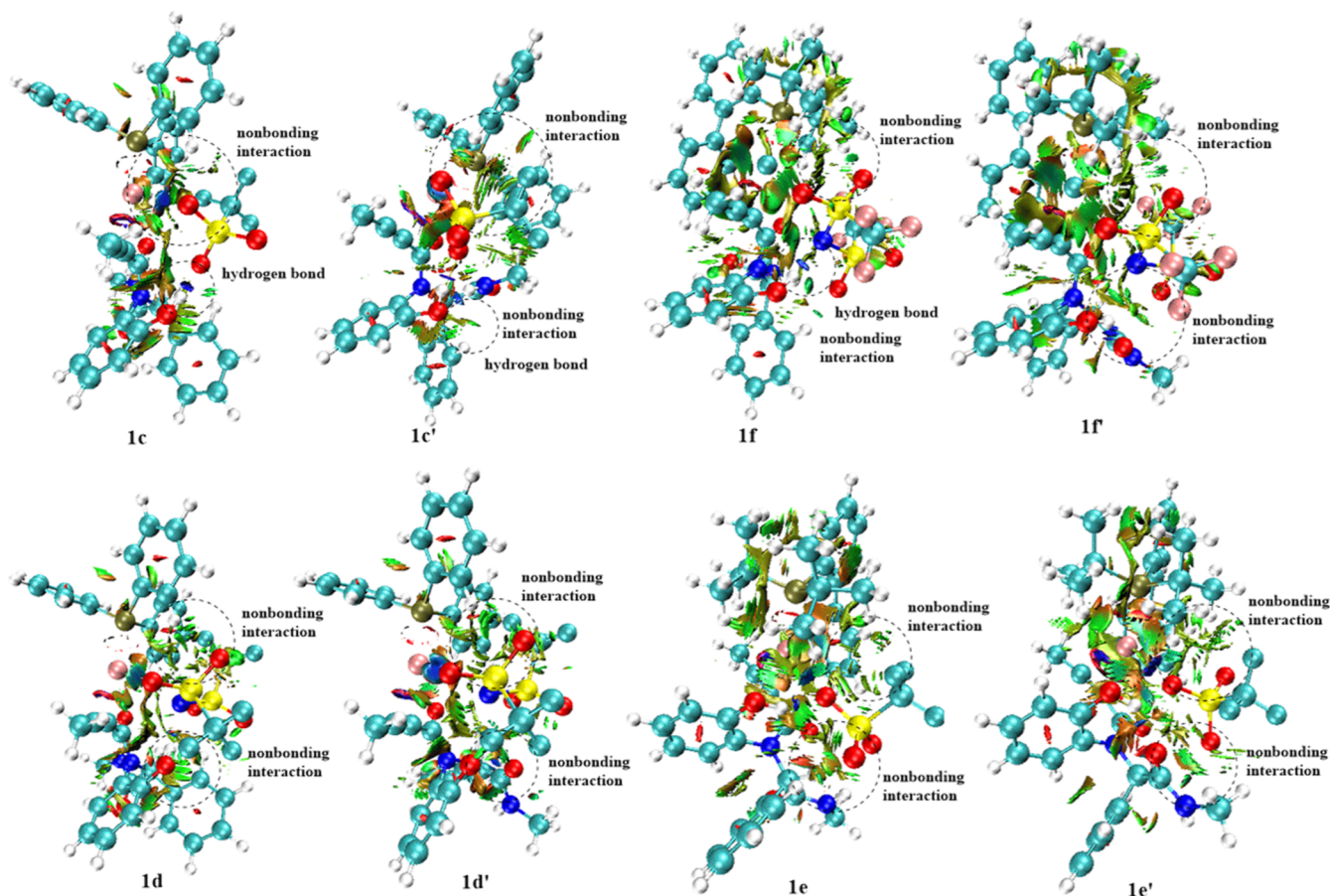
Figure 4. Noncovalent interaction analyses (NCI) for diastereoselectivity-determining transition states in the gold complex-catalyzed reaction. Blue, green, and red surfaces represent the strong interaction, weak interaction, and steric effect, respectively.
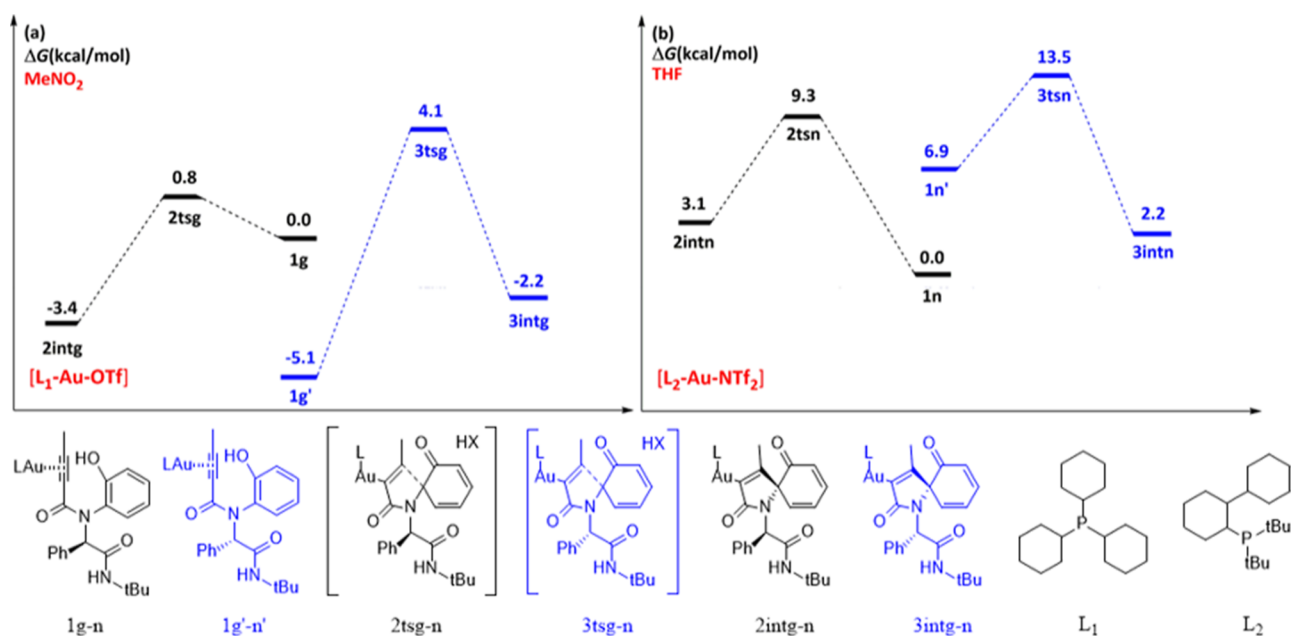

Figure 5. Gibbs free energy profiles of spiro cyclization with different ligands, counterions, and solvent. (a) **g**: Ligands: PPh$_3$, counterions: OTf$^-$, solvent/MeNO$_2$; (b) **n**: ligands: JohnPhos, counterions: NTf$_2^-$, solvent/THF. **1g−n** and **1g′−n′** are reactants. **2tsg-n** and **3tsg-n** are reaction transition states. **2intg-n** and **3intg-n** are reaction intermediates.

between ligands and counterions on the diastereoselectivity switch. From the energy profiles above, it seems that the cooperation between counterions and ligands play a substantial

role in the divergent diastereoselectivity. Therefore, we have elucidated the origin of gold-catalyzed post-Ugi ipso-cyclization with switchable diastereoselectivity. The choice of

the gold complex is key for the diastereoselectivity of this ipso-cyclization. With the combination of PPh₃PAuCl and AgOTf as the catalyst, the reaction preferred **3a** (Scheme 1). However, when it came to the combination of JohnPhosAuCl and AgNTf₂, the reaction diastereoselectivity switch turned to afford **2a** (Scheme 1). The diastereoselectivity switch might be derived from the differences of electron population and steric hindrance in the alkyne activated by gold catalysts. As shown in Figure 2a, the energy barrier difference between **1c** and **1c′** is 8.0 kcal/mol, and the product **3a** (Scheme 1) was exclusively achieved with the assistance of the rigid electron-abundant PPh₃ ligand and counterion OTf⁻. As shown in Figure 2b, the calculated energy barrier difference between **1f** and **1f′** is −9.1 kcal/mol. Obviously, this indicated that synergy of the ligands and counterions should be responsible for the observed diastereoselectivity switch.

We believe that further exploration of the factors affecting the reaction outcome, such as ligand, counterion, solvent, and temperature, represents a highly promising direction for catalyst design. The new stereochemical model is consistent with the observed experimental results in terms of selectivity and levels of diastereo-control as catalytic system. It also sheds light on the synergistic effect between ligand and counterion on stereoinduction.

Solvation Correction. After solvation correction (Figure 5), it is found that the two optimal conditions are **g** (triphenylphosphine as the ligand, OTf⁻ as the counterion, and MeNO₂ as the solvent) and **n** (using the JohnPhos ligand, NTf₂⁻ as the counterion, and THF as the solvent). The energy barrier difference between the two conformations **1g** and **1g′** is 5.1 kcal/mol (Figure 5a). In addition, the energy barrier difference between the two conformations **1n** and **1n′** is −6.9 kcal/mol (Figure 5b). The solvent has a significant effect on the energy of reactants and transition states, but it does not change the direction of diastereoselectivity of the reaction.

CONCLUSIONS

The origins of the diastereoselectivity switch of gold-catalyzed post-Ugi ipso-cyclization synthesis of the spirocyclic pyrrol-2-one-dione system have been theoretically explored for the first time. The choice of the gold complex is shown to be an important factor for the diastereoselectivity switch onto this system. The synergistic effect by both ligand and counterion was found to play a key role in the diastereoselectivity switch. In contrast to previous computational results on gold-catalyzed domino cyclization, it has been shown that nonbonding interactions between substrate and ligand or counterions are responsible for the stabilization of reactants and the diastereoselectivity switch. Our results shed light on the synergistic effects of ligand and counterion on gold complex on stereo-induction. Systematic studies of other types of gold-catalyzed asymmetric dearomatizing spiro-cyclizations are also ongoing in our group and will be reported in due course.

ASSOCIATED CONTENT

Ⓢ Supporting Information

The Supporting Information is available free of charge at https://pubs.acs.org/doi/10.1021/acsomega.3c01279.

Relative energies, single-point energy profiles, relative concentrations, spin density maps, structures for BCPs, BCP parameters, TDOS and PDOS, SOMO/HOMO− LUMO gaps and maps, and Cartesian coordinates of M₂O@C₈₀ (M = Sc or Gd) (PDF)

AUTHOR INFORMATION

Corresponding Author

Xiang Zhao − *Institute of Molecular Science and Applied Chemistry, School of Chemistry, State Key Laboratory of Electrical Insulation and Power Equipment & MOE Key Laboratory for Nonequilibrium Synthesis and Modulation of Condensed Matter, Xi'an Jiaotong University, Xi'an 710049, China;* ● orcid.org/0000-0003-3982-4763; Email: xzhao@mail.xjtu.edu.cn

Authors

Jun He − *Institute of Molecular Science and Applied Chemistry, School of Chemistry, State Key Laboratory of Electrical Insulation and Power Equipment & MOE Key Laboratory for Nonequilibrium Synthesis and Modulation of Condensed Matter, Xi'an Jiaotong University, Xi'an 710049, China*

Jie Zhang − *Institute of Molecular Science and Applied Chemistry, School of Chemistry, State Key Laboratory of Electrical Insulation and Power Equipment & MOE Key Laboratory for Nonequilibrium Synthesis and Modulation of Condensed Matter, Xi'an Jiaotong University, Xi'an 710049, China*

Yunhe Li − *School of Materials Science and Engineering, Lanzhou Jiaotong University, Lanzhou 730070, China*

Yan-bo Han − *Institute of Molecular Science and Applied Chemistry, School of Chemistry, State Key Laboratory of Electrical Insulation and Power Equipment & MOE Key Laboratory for Nonequilibrium Synthesis and Modulation of Condensed Matter, Xi'an Jiaotong University, Xi'an 710049, China*

Mengyang Li − *School of Physics, Xidian University, Xi'an 710071, China*

Complete contact information is available at:
https://pubs.acs.org/10.1021/acsomega.3c01279

Author Contributions

‖J.H., J.Z. and Y.L. contributed equally to this work.

Notes

The authors declare no competing financial interest.

REFERENCES

(1) He, Y.; Song, L.; Liu, C.; Wu, D.; Li, Z.; Van Meervelt, L.; Van der Eycken, E. V. Access to Polycyclic Azepino[5,4,3-cd]indoles via a Gold-Catalyzed Post-Ugi Dearomatization Cascade. *J. Org. Chem.* **2020**, *85*, 15092−15103.

(2) Fedoseev, P.; Coppola, G.; Ojeda, G. M.; Van der Eycken, E. V. Synthesis of spiroindolenines by intramolecular ipso-iodocyclization of indol ynones. *Chem. Commun.* **2018**, *54*, 3625−3628.

(3) He, Y.; Liu, Z.; Wu, D. J.; Li, Z. H.; Robeyns, K.; Van Meervelt, L.; Van der Eycken, E. V. Modular Access to Diverse Bridged Indole Alkaloid Mimics via a Gold-Triggered Cascade Dearomative Spirocarbocyclization/[4+2] Cycloaddition Sequence. *Org. Lett.* **2019**, *21*, 4469−4474.

(4) Zheng, C.; You, S. L. Catalytic asymmetric dearomatization (CADA) reaction-enabled total synthesis of indole-based natural products. *Nat. Prod. Rep.* **2019**, *36*, 1589−1605.

(5) Zheng, J.; Wang, S. B.; Zheng, C.; You, S. L. Asymmetric Dearomatization of Naphthols via a Rh-Catalyzed C(sp(2))-H Functionalization/Annulation Reaction. *J. Am. Chem. Soc.* **2015**, *137*, 4880−4883.

(6) Ding, L.; You, S. L. Palladium(0)-Catalyzed Intermolecular Cascade Dearomatization Reaction of beta-Naphthol Derivatives with Propargyl Carbonates. *Org. Lett.* **2018**, *20*, 6206−6210.

(7) An, J. Z.; Lombardi, L.; Grilli, S.; Bandini, M. PPh(3)AuTFA Catalyzed in the Dearomatization of 2-Naphthols with Allenamides. *Org. Lett.* **2018**, *20*, 7380−7383.

(8) Zheng, C.; You, S. L. Advances in Catalytic Asymmetric Dearomatization. *ACS Cent. Sci.* **2021**, *7*, 432−444.

(9) Wu, L. L.; Sheong, F. K.; Lin, Z. Y. DFT Studies on Copper-Catalyzed Dearomatization of Pyridine. *ACS Catal.* **2020**, *10*, 9585−9593.

(10) Gatto, M.; Baratta, W.; Belanzoni, P.; Belpassi, L.; Del Zotto, A.; Tarantelli, F.; Zuccaccia, D. Hydration and alkoxylation of alkynes catalyzed by NHC-Au-OTf. *Green Chem.* **2018**, *20*, 2125−2134.

(11) Wang, Y. L.; Zheng, Z. T.; Zhang, L. M. Intramolecular Insertions into Unactivated C(sp(3))-H Bonds by Oxidatively Generated beta-Diketone-alpha-Gold Carbenes: Synthesis of Cyclopentanones. *J. Am. Chem. Soc.* **2015**, *137*, 5316−5319.

(12) Wang, Y. L.; Yepremyan, A.; Ghorai, S.; Todd, R.; Aue, D. H.; Zhang, L. M. Gold-Catalyzed Cyclizations of cis-Enediynes: Insights into the Nature of Gold-Aryne Interactions. *Angew. Chem., Int. Ed.* **2013**, *52*, 7795−7799.

(13) Jia, M. Q.; Bandini, M. Counterion Effects in Homogeneous Gold Catalysis. *ACS Catal.* **2015**, *5*, 1638−1652.

(14) Mandal, N.; Datta, A. Gold(I)-Catalyzed Intramolecular Diels−Alder Reaction: Evolution of Trappable Intermediates via Asynchronous Transition States. *J. Org. Chem.* **2018**, *83*, 11167−11177.

(15) Brenzovich, W. E., Jr.; Benitez, D.; Lackner, A. D.; Shunatona, H. P.; Tkatchouk, E.; Goddard, W. A., III; Toste, F. D. Gold-Catalyzed Intramolecular Aminoarylation of Alkenes: C C Bond Formation through Bimolecular Reductive Elimination. *Angew. Chem., Int. Ed.* **2010**, *49*, 5519−5522.

(16) Bhattacharjee, R.; Nijamudheen, A.; Datta, A. Direct and Autocatalytic Reductive Elimination from Gold Complexes ([(Ph3P)-Au(Ar)(CF3)(X)], X=F, Cl, Br, I): The Key Role of Halide Ligands. *Chem.—Eur. J.* **2017**, *23*, 4169−4179.

(17) Nijamudheen, A.; Jose, D.; Datta, A. Why Does Gold(III) Porphyrin Act as a Selective Catalyst in the Cycloisomerization of Allenones? *J. Phys. Chem. C* **2011**, *115*, 2187−2195.

(18) Yang, Y. Y.; Li, J. H.; Zhu, R. X.; Liu, C. B.; Zhang, D. J. Theoretical Insight into Ligand- and Counterion-Controlled Regiodivergent Reactivity in Synthesis of Borylated Furans: 1,2-H vs 1,2-B Migration. *ACS Catal.* **2018**, *8*, 9252−9261.

(19) Yang, Y. Y.; Liu, Y. H.; Zhu, R. X.; Zhang, D. J. Theoretical Insight into Palladium(II)-Counterion-Ligand Cooperative Regiodivergent Syntheses of Indolo[3,2-c]coumarins and Benzofuro[3,2-c]quinolinones from Diphenylethyne Derivatives. *Inorg. Chem.* **2020**, *59*, 4741−4752.

(20) Yang, Y. Y.; Li, J. H.; Zhu, R. X.; Liu, C. B.; Zhang, D. J. Theoretical Insight into the Au(I)-Catalyzed Intermolecular Condensation of Homopropargyl Alcohols with Terminal Alkynes: Reactant Stoichiometric Ratio-Controlled Chemodivergence. *J. Org. Chem.* **2019**, *84*, 579−588.

(21) Sabat, N.; Soualmia, F.; Retailleau, P.; Benjdia, A.; Berteau, O.; Guinchard, X. Gold-Catalyzed Spirocyclization Reactions of N-Propargyl Tryptamines and Tryptophans in Aqueous Media. *Org. Lett.* **2020**, *22*, 4344−4349.

(22) Crawford, J. M.; Kingston, C.; Toste, F. D.; Sigman, M. S. Data Science Meets Physical Organic Chemistry. *Acc. Chem. Res.* **2021**, *54*, 3136−3148.

(23) Shoja, A.; Zhai, J.; Reid, J. P. Comprehensive Stereochemical Models for Selectivity Prediction in Diverse Chiral Phosphate-Catalyzed Reaction Space. *ACS Catal.* **2021**, *11*, 11897−11905.

(24) Becker, M. R.; Reid, J. P.; Rykaczewski, K. A.; Schindler, C. S. Models for Understanding Divergent Reactivity in Lewis Acid-Catalyzed Transformations of Carbonyls and Olefins. *ACS Catal.* **2020**, *10*, 4387−4397.

(25) Maji, R.; Mallojjala, S. C.; Wheeler, S. E. Chiral phosphoric acid catalysis: from numbers to insights. *Chem. Soc. Rev.* **2018**, *47*, 1142−1158.

(26) Durand, D. J.; Fey, N. Building a Toolbox for the Analysis and Prediction of Ligand and Catalyst Effects in Organometallic Catalysis. *Acc. Chem. Res.* **2021**, *54*, 837−848.

(27) Sharma, U. K.; Ranjan, P.; Van der Eycken, E. V.; You, S. L. Sequential and direct multicomponent reaction (MCR)-based dearomatization strategies. *Chem. Soc. Rev.* **2020**, *49*, 8721−8748.

(28) Modha, S. G.; Kumar, A.; Vachhani, D. D.; Sharma, S. K.; Parmar, V. S.; Van der Eycken, E. V. Gold(I) and platinum(II) switch: a post-Ugi intramolecular hydroarylation to pyrrolopyridinones and pyrroloazepinones. *Chem. Commun.* **2012**, *48*, 10916−10918.

(29) Modha, S. G.; Kumar, A.; Vachhani, D. D.; Jacobs, J.; Sharma, S. K.; Parmar, V. S.; Van Meervelt, L.; Van der Eycken, E. V. A Diversity-Oriented Approach to Spiroindolines: Post-Ugi Gold-Catalyzed Diastereoselective Domino Cyclization. *Angew. Chem., Int. Ed.* **2012**, *51*, 9572−9575.

(30) He, Y.; Li, Z. H.; Tian, G. L.; Song, L. L.; Van Meervelt, L.; Van der Eycken, E. V. Gold-catalyzed diastereoselective domino dearomatization/ipso-cyclization/aza-Michael sequence: a facile access to diverse fused azaspiro tetracyclic scaffolds. *Chem. Commun.* **2017**, *53*, 6413−6416.

(31) Li, Y. H.; Zhao, X. Mechanism and origins of gold-catalyzed domino cyclization to spiroindolines: the role of periplanar cooperation and hydrogen bonding interactions. *Org. Chem. Front.* **2020**, *7*, 1663−1670.

(32) Li, Y. H.; Zhao, X. Gold-catalyzed domino cyclization enabling construction of diverse fused azaspiro tetracyclic scaffolds: a cascade catalysis mechanism due to a substrate and counterion. *Catal. Sci. Technol.* **2020**, *10*, 2415−2426.

(33) Nechaev, A. A.; Van Hecke, K.; Zaman, M.; Kashtanov, S.; Ungur, L.; Pereshivko, O. P.; Peshkov, V. A.; Van der Eycken, E. V. Gold-Catalyzed Post-Ugi Ipso-Cyclization with Switchable Diastereoselectivity. *J. Org. Chem.* **2018**, *83*, 8170−8182.

(34) Singh, K.; Malviya, B. K.; Roy, T. K.; Mithu, V. S.; Bhardwaj, V. K.; Verma, V. P.; Chimni, S. S.; Sharma, S. Catalyst-Controlled Structural Divergence: Selective Intramolecular 7-endo-dig and 6-exo-dig Post-Ugi Cyclization for the Synthesis of Benzoxazepinones and Benzoxazinones. *J. Org. Chem.* **2018**, *83*, 57−68.

(35) Wu, W. T.; Xu, R. Q.; Zhang, L. M.; You, S. L. Construction of spirocarbocycles via gold-catalyzed intramolecular dearomatization of naphthols. *Chem. Sci.* **2016**, *7*, 3427−3431.

(36) He, Y.; Li, Z. H.; Robeyns, K.; Van Meervelt, L.; Van der Eycken, E. V. A Gold-Catalyzed Domino Cyclization Enabling Rapid Construction of Diverse Polyheterocyclic Frameworks. *Angew. Chem., Int. Ed.* **2018**, *57*, 272−276.

(37) Lu, Z. C.; Han, J. B.; Okoromoba, O. E.; Shimizu, N.; Amii, H.; Tormena, C. F.; Hammond, G. B.; Xu, B. Predicting Counterion Effects Using a Gold Affinity Index and a Hydrogen Bonding Basicity Index. *Org. Lett.* **2017**, *19*, 5848−5851.

(38) Li, F.; Korenaga, T.; Nakanishi, T.; Kikuchi, J.; Terada, M. Chiral Phosphoric Acid Catalyzed Enantioselective Ring Expansion Reaction of 1,3-Dithiane Derivatives: Case Study of the Nature of Ion-Pairing Interaction. *J. Am. Chem. Soc.* **2018**, *140*, 2629−2642.

(39) Balcells, D.; Clot, E.; Eisenstein, O.; Nova, A.; Perrin, L. Deciphering Selectivity in Organic Reactions: A Multifaceted Problem. *Acc. Chem. Res.* **2016**, *49*, 1070−1078.

(40) Wang, Y.; Qu, L. B.; Lan, Y.; Wei, D. H. Origin of Regio- and Stereoselectivity in the NHC-catalyzed Reaction of Alkyl Pyridinium with Aliphatic Enal. *ChemCatChem* **2020**, *12*, 1068−1074.

(41) Sigman, M. S.; Harper, K. C.; Bess, E. N.; Milo, A. The Development of Multidimensional Analysis Tools for Asymmetric Catalysis and Beyond. *Acc. Chem. Res.* **2016**, *49*, 1292−1301.

(42) Wu, W. T.; Zhang, L. M.; You, S. L. Catalytic asymmetric dearomatization (CADA) reactions of phenol and aniline derivatives. *Chem. Soc. Rev.* **2016**, *45*, 1570−1580.

(43) Lam, Y. H.; Grayson, M. N.; Holland, M. C.; Simon, A.; Houk, K. N. Theory and Modeling of Asymmetric Catalytic Reactions. *Acc. Chem. Res.* **2016**, *49*, 750−762.

(44) Frisch, M. J.; Trucks, G. W.; Schlegel, H. B.; Scuseria, G. E.; Robb, M. A.; Cheeseman, J. R.; Scalmani, G.; Barone, V.; Petersson, G. A.; Nakatsuji, H.; Li, X.; Caricato, M.; Marenich, A. V.; Bloino, J.; Janesko, B. G.; Gomperts, R.; Mennucci, B.; Hratchian, H. P.; Ortiz, J. V.; Izmaylov, A. F.; Sonnenberg, J. L.; Ding, F.; Lipparini, F.; Egidi, F.; Goings, J.; Peng, B.; Petrone, A.; Henderson, T.; Ranasinghe, D.; Zakrzewski, V. G.; Gao, J.; Rega, N.; Zheng, G.; Liang, W.; Hada, M.; Ehara, M.; Toyota, K.; Fukuda, R.; Hasegawa, J.; Ishida, M.; Nakajima, T.; Honda, Y.; Kitao, O.; Nakai, H.; Vreven, T.; Throssell, K.; Montgomery, J. A., Jr.; Peralta, J. E.; Ogliaro, F.; Bearpark, M. J.; Heyd, J. J.; Brothers, E. N.; Kudin, K. N.; Staroverov, V. N.; Keith, T. A.; Kobayashi, R.; Normand, J.; Raghavachari, K.; Rendell, A. P.; Burant, J. C.; Iyengar, S. S.; Tomasi, J.; Cossi, M.; Millam, J. M.; Klene, M.; Adamo, C.; Cammi, R.; Ochterski, J. W.; Martin, R. L.; Morokuma, K.; Farkas, O.; Foresman, J. B.; Fox, D. J. *Gaussian 16*; Rev. B.01; Gaussian, Inc.: Wallingford, CT, 2016.

(45) Huzinaga, S. Basis-sets for molecular calculations. *CoPhR* **1985**, *2*, 281−339.

(46) Ribeiro, R. F.; Marenich, A. V.; Cramer, C. J.; Truhlar, D. G. Use of Solution-Phase Vibrational Frequencies in Continuum Models for the Free Energy of Solvation. *J. Phys. Chem. B* **2011**, *115*, 14556−14562.

(47) Fukui, K. The path of chemical reactions - the IRC approach. *Acc. Chem. Res.* **1981**, *14*, 363−368.

(48) Fukui, K. Formulation of the reaction coordinate. *J. Phys. Chem.* **1970**, *74*, 4161−4163.

(49) Legault, C. Y. *CYLview, 1.0B*; Universite de Sherbrooke: Quebec, Canda, 2009. http://www.cylview.org.

(50) Lu, T.; Chen, F. W. Multiwfn: A multifunctional wavefunction analyzer. *J. Comput. Chem.* **2012**, *33*, 580−592.

(51) Humphrey, W.; Dalke, A.; Schulten, K. VMD: Visual molecular dynamics. *J. Mol. Graph. Model.* **1996**, *14*, 33−38.

(52) te Velde, G.; Bickelhaupt, F. M.; Baerends, E. J.; Fonseca Guerra, C.; Van Gisbergen, S. J. A.; Snijders, J. G.; Ziegler, T. Chemistry with ADF. *J. Comput. Chem.* **2001**, *22*, 931−967.

(53) Changotra, A.; Das, S.; Sunoj, R. B. Reversing Enantiose-lectivity Using Noncovalent Interactions in Asymmetric Dearomatiza-tion of beta-Naphthols: The Power of 3,3 ' Substituents in Chiral Phosphoric Acid Catalysts. *Org. Lett.* **2017**, *19*, 2354−2357.

(54) Zhao, Y.; Truhlar, D. G. Density functionals with broad applicability in chemistry. *Acc. Chem. Res.* **2008**, *41*, 157−167.

(55) Zhao, Y.; Truhlar, D. G. The M06 suite of density functionals for main group thermochemistry, thermochemical kinetics, non-covalent interactions, excited states, and transition elements: two new functionals and systematic testing of four M06-class functionals and 12 other functionals. *Theor. Chem. Acc.* **2008**, *120*, 215−241.